

Muon polarization in the MEG experiment: predictions and measurements

The MEG Collaboration

A. M. Baldini ^{4a}, Y. Bao ¹, E. Baracchini ^{3‡}, C. Bemporad ^{4ab}, F. Berg ^{1,2}, M. Biasotti ^{8ab},
G. Boca ^{6ab}, P.W. Cattaneo ^{6a}, G. Cavoto ^{7a}, F. Ceci ^{4ab*}, G. Chiarello ^{13ab}, C. Chiri ^{13ab},
A. De Bari ^{6ab}, M. De Gerone ^{8a}, A. D’Onofrio ^{4ab}, S. Dussoni ^{4a}, Y. Fujii ³, L. Galli ^{4a},
F. Gatti ^{8ab}, F. Grancagnolo ^{13a}, M. Grassi ^{4a}, A. Graziosi ^{7ab}, D.N. Grigoriev ^{10,14,15},
T. Haruyama ¹¹, M. Hildebrandt ¹, Z. Hodge ^{1,2}, K. Ieki ^{1,3}, F. Ignatov ^{10,15}, T. Iwamoto ³,
D. Kaneko ³, T.I. Kang ⁵, P.-R. Kettle ¹, B.I. Khazin ^{10,15†}, N. Khomutov ¹²,
A. Korenchenko ¹², N. Kravchuk ¹², G.M.A. Lim ⁵, S. Mihara ¹¹, W. Molzon ⁵,
Toshinori Mori ³, A. Mtchedlishvili ¹, S. Nakaura ³, D. Nicolò ^{4ab}, H. Nishiguchi ¹¹,
M. Nishimura ³, S. Ogawa ³, W. Ootani ³, M. Panareo ^{13ab}, A. Papa ¹, A. Pepino ^{13ab},
G. Piredda ^{7a}, G. Pizzigoni ^{8ab}, A. Popov ^{10,15}, F. Renga ^{7a}, E. Ripiccini ^{7ab}, S. Ritt ¹,
M. Rossella ^{6a}, G. Rutar ^{1,2}, R. Sawada ³, F. Sergiampietri ^{4a}, G. Signorelli ^{4a},
G. Tassielli ^{13a}, F. Tenchini ^{4ab}, Y. Uchiyama ³, M. Venturini ^{4ac}, C. Voena ^{7a},
A. Yamamoto ¹¹, K. Yoshida ³, Z. You ⁵, Yu.V. Yudin ^{10,15},

¹ Paul Scherrer Institut PSI, CH-5232, Villigen, Switzerland

² Swiss Federal Institute of Technology ETH, CH-8093 Zürich, Switzerland

³ ICEPP, University of Tokyo 7-3-1 Hongo, Bunkyo-ku, Tokyo 113-0033, Japan

⁴ INFN Sezione di Pisa^a; Dipartimento di Fisica^b dell’Università, Largo B. Pontecorvo 3, 56127 Pisa, Italy

⁵ University of California, Irvine, CA 92697, USA

⁶ INFN Sezione di Pavia^a; Dipartimento di Fisica^b dell’Università, Via Bassi 6, 27100 Pavia, Italy

⁷ INFN Sezione di Roma^a; Dipartimento di Fisica^b dell’Università “Sapienza”, Piazzale A. Moro, 00185 Roma, Italy

⁸ INFN Sezione di Genova^a; Dipartimento di Fisica^b dell’Università, Via Dodecaneso 33, 16146 Genova, Italy

⁹ Research Institute for Science and Engineering, Waseda University, 3-4-1 Okubo, Shinjuku-ku, Tokyo 169-8555, Japan

¹⁰ Budker Institute of Nuclear Physics of Siberian Branch of Russian Academy of Sciences, 630090, Novosibirsk, Russia

¹¹ KEK, High Energy Accelerator Research Organization 1-1 Oho, Tsukuba, Ibaraki, 305-0801, Japan

¹² Joint Institute for Nuclear Research, 141980, Dubna, Russia

¹³ INFN Sezione di Lecce^a; Dipartimento di Matematica e Fisica^b dell’Università, Via per Arnesano, 73100 Lecce, Italy

¹⁴ Novosibirsk State Technical University, 630092, Novosibirsk, Russia

¹⁵ Novosibirsk State University, 630090 Novosibirsk, Russia

Received: date / Accepted: date

Abstract The MEG experiment makes use of one of the world’s most intense low energy muon beams, in order to search for the lepton flavour violating process $\mu^+ \rightarrow e^+ \gamma$. We determined the residual beam polarization at the thin stopping target, by measuring the asymmetry of the angular distribution of Michel decay positrons as a function of energy. The initial muon beam polarization at the production is predicted to be $P_\mu = -1$ by the Standard Model (SM) with massless neutrinos. We estimated our residual muon polarization to be $P_\mu = -0.85 \pm 0.03$ (stat) $^{+0.04}_{-0.05}$ (syst) at the stopping target, which is consistent with the SM pre-

dictions when the depolarizing effects occurring during the muon production, propagation and moderation in the target are taken into account. The knowledge of beam polarization is of fundamental importance in order to model the background of our $\mu^+ \rightarrow e^+ \gamma$ search induced by the muon radiative decay: $\mu^+ \rightarrow e^+ \bar{\nu}_\mu \nu_e \gamma$.

1 Introduction

Low energy muon physics experiments frequently use copious beams of “surface muons”, i.e. muons generated by pions decaying at rest close to the surface of the pion production target, such as those produced at meson factories (PSI and TRIUMF). In the Standard Model (SM) with massless neutrinos, positive (negative) muons are fully polarized,

*Corresponding author: fabrizio.cei@pi.infn.it

†Deceased.

‡Presently at INFN, Laboratori Nazionali di Frascati, via E.Fermi, 40, 00044 Frascati (Roma) Italy

with the spin opposite (parallel) to the muon momentum vector, that is $P_\mu = -1$ for positive muons, at the production point; the muon polarization can be partially reduced by the muon interaction with the electric and magnetic fields of the muon beam line as well as with the muon stopping target. The degree of polarization at the muon decay point affects both the energy and angular distribution of the muon decay products i.e. Michel positrons and γ 's from the normal $\mu^+ \rightarrow e^+ \nu \bar{\nu}$ and radiative muon decay $\mu^+ \rightarrow e^+ \bar{\nu}_\mu \nu_e \gamma$. The muon decay products are an important background when searching for rare decays such as $\mu^+ \rightarrow e^+ \gamma$; a precise knowledge of their distribution is therefore mandatory. We report on the determination of the residual muon polarization in the PSI $\pi E5$ PE5 channel and MEG beam line Adam et al. [2013a] from the data collected by the MEG experiment between 2009 and 2011. Clear signs of the muon polarization are visible in the Michel positron angular distribution; the measured polarization is in good agreement with a theoretical calculation (see Section 2) based on the SM predictions and on the beam line characteristics.

The MEG experiment at the Paul Scherrer Institute (PSI) PSI has been searching for the lepton flavour violating decay $\mu^+ \rightarrow e^+ \gamma$ since 2008. Preliminary results were published in Adam et al. [2010, 2011a] and Adam et al. [2013b]. The analysis of the MEG full data sample is under way and will soon be published. A detailed description of the experiment can be found in Adam et al. [2013a]. A high intensity surface muon beam ($\sim 3 \times 10^7 \mu^+/s$), from the $\pi E5$ channel and MEG beam line, is brought to rest in a 205 μm slanted plastic target, placed at the centre of the experimental set-up. The muon decay products are detected by a spectrometer with a gradient magnetic field and by an electromagnetic calorimeter. The magnetic field is generated by a multi-coil superconducting magnet (COBRA) Yamamoto et al. [2002], Ootani et al. [2004], with conventional compensation coils; the maximum intensity of the field is 1.26 T at the target position. The positron momenta are measured by sixteen drift chambers (DCH) Hildebrandt [2010], radially aligned, and their arrival times by means of a Timing Counter (TC) S. Dussoni and M. De Gerone and F. Gatti and R. Valle and M. [2010], De Gerone et al. [2012, 2011], consisting of two scintillator arrays, placed at opposite sides relative to the muon target. The momentum vector and the arrival time of photons are measured in a 900 liter C-shaped liquid xenon photon detector (LXe) Sawada [2010], Mihara [2011], equipped with a dense array of 846 UV-sensitive PMTs. A dedicated trigger system Galli et al. [2013, 2014] allows an efficient preselection of possible $\mu^+ \rightarrow e^+ \gamma$ candidates, with an almost zero dead-time. The signals coming from the DCH, TC and LXe detectors are processed by a custom-made waveform digitizer system (DRS4) Ritt [2004], Ritt et al. [2010] operating at a maximum sampling speed close to 2 GHz. Several calibration tools are in operation, allowing a con-

tinuous monitoring of the experiment Baldini et al. [2006], Adam et al. [2011b]. Dedicated prescaled trigger schemes collect calibration events for a limited amount of time (few hours/week). A complete list of the experimental resolutions (σ 's) for energies close to the kinematic limit $m_\mu/2$ can be found in Adam et al. [2013b]; the most relevant being: ~ 340 keV/c for the positron momentum, ~ 10 mrad for the positron zenith angle and ~ 1 and ~ 3 mm for the positron vertex along the two axes orthogonal to the beam direction.

The beam axis defines the z -axis of the MEG reference frame. The part of the detector preceeding the muon target is called the “UpStream” (US) side and that following the muon target is called the “DownStream” (DS) side. The θ zenith angle range of the apparatus is ($(\approx 60^\circ) - 90^\circ$) on the DS-side and ($90^\circ - (\approx 120^\circ)$) on the US-side. The SM prediction is $P_\mu^z = -1$ for muons travelling along the positive z -axis.

2 Theoretical issues

The $\pi E5$ channel is a high-intensity low-energy pion and muon beam line in the $10 \text{ MeV}/c < p < 120 \text{ MeV}/c$ momentum range. Surface muons have a kinetic energy of 4.12 MeV and a muon momentum of $\approx 29.79 \text{ MeV}/c$ and are produced fully polarized along the direction opposite to their momentum vector. Several depolarizing effects can reduce the effective polarization along the beam line. They are classified into three groups:

- 1) effects at the production stage, close to and within the production target;
- 2) effects along the beam line up to the stopping target;
- 3) effects during the muon moderation and stopping process in the target.

2.1 Depolarization at the production stage

Since the angular divergence of the beam is not zero, the average muon polarization P_μ^z along the muon flight direction does not coincide with P_μ^z where z is the direction of the muon beam (the beam acceptance at the source is 150 msr and the angular divergence is 450 mrad in the horizontal and 120 mrad in the vertical direction).

One such depolarizing effect is due to the multiple scattering in the target, which modifies the muon direction leaving the spin unaffected. Surface muons have a maximum range in the carbon production target of 0.82 mm. The average broadening angle due to multiple scattering is then given by (see for instance Ritt [1976]):

$$\langle \cos \alpha \rangle = 1 - 21 \frac{x}{X_0} \left[\left(\frac{30}{P} \right)^{0.5} - 1 \right] \quad (1)$$

where P is the muon momentum in MeV/ c and x/X_0 is the muon path in the target in units of carbon radiation lengths ($X_0 = 18.8$ cm). We obtain $\langle \cos \alpha \rangle = 0.997$, a contribution of less than 0.5 %.

A more important effect is due to “cloud muons”, i.e. muons originating from pion decays in flight, in or close to the production target, and accepted by the beam transport system. These muons have only a small net polarization due to their differing acceptance kinematics which leads to an overall reduction of the beam polarization, based on studies performed at LAMPF Van Dyck et al. [1979] and measurements we made at the $\pi E5$ channel at PSI. The latter involved the fitting of a constant cloud muon content to the limited region of the measured muon momentum spectrum, around the kinematic edge at ≈ 29.79 MeV/ c . This was cross-checked by direct measurements of negative cloud muons at the MEG central beam momentum of 28 MeV/ c , where there is no surface muon contribution on account of the charge sign (muonic atom formation of stopped negative muons). The cloud muon content was found to be consistent from both measurements when taking the kinematics and cross-sections of positive and negative pions into account. This leads to an estimated depolarization of $(4.5 \pm 1.5 \%)$, which is the single-most important effect at the production stage.

2.2 Depolarization along the beam line

The MEG beam line comprises of several different elements: quadrupole and bending magnets, fringing fields, an electrostatic separator, a beam transport solenoid and the COBRA spectrometer. The equation of motion of the muon spin \mathbf{s} is described, even in a spatially varying magnetic field such as the COBRA spectrometer, by the Thomas equation Jackson [1998]:

$$\frac{d\mathbf{s}}{dt} = \frac{e}{mc} \mathbf{s} \times \left[\left(\frac{g}{2} - 1 + \frac{1}{\gamma} \right) \mathbf{B} - \left(\frac{g}{2} - 1 \right) \frac{\gamma}{\gamma + 1} (\boldsymbol{\beta} \cdot \mathbf{B}) \boldsymbol{\beta} - \left(\frac{g}{2} - \frac{\gamma}{\gamma + 1} \right) \boldsymbol{\beta} \times \mathbf{E} \right] \quad (2)$$

where $\boldsymbol{\beta}$, e and m are the muon velocity, electric charge and mass, c is the speed of light, $\gamma = 1/\sqrt{1-\beta^2}$, g is the muon gyromagnetic factor and \mathbf{B} and \mathbf{E} are the electric and magnetic field vectors. In principle this equation is valid only for uniform fields, but it gives correct results even in our case since any effect due to the non-uniformity of the magnetic field is many orders of magnitude smaller than the Lorentz force in the weak gradient field of COBRA. From equation (2) we can obtain the time evolution of the longitudinal polarization, defined as the projection of the spin vector along the momentum vector, which is given by:

$$\frac{d(\mathbf{s} \cdot \boldsymbol{\beta})}{dt} = -\frac{e}{mc} \mathbf{s}_\perp \cdot \left[\left(\frac{g}{2} - 1 \right) \boldsymbol{\beta} \times \mathbf{B} + \left(\frac{g\boldsymbol{\beta}}{2} - \frac{1}{\boldsymbol{\beta}} \right) \mathbf{E} \right] \quad (3)$$

where \mathbf{s}_\perp is the projection of the spin vector in the plane orthogonal to the muon momentum. In this equation, the first contribution is due to the muon magnetic moment anomaly ($\frac{g-2}{2} \approx \frac{\alpha}{2\pi}$) and the second to the presence of an electric field. In the MEG beam line the first term is associated with the guiding elements (quadrupole and bending magnets), while the second term is associated with the electrostatic separator. The geometrical parameters of the beam elements and their field intensities are PE5: for the deflecting magnets the length is ≈ 70 cm and the vertical field is ≈ 0.15 T; for the electrostatic separator the length is 82 cm, the gap between the plates 19 cm and the applied voltage -195 kV. The COBRA spectrometer has a weak spatially varying magnetic field, which muons are subjected to while travelling on the US-side of the magnet, after being focused by the beam transport solenoid; the average vertical component of the COBRA magnetic field around the muon trajectory is of order of 0.025 T and its contribution to the spin rotation is about one order of magnitude smaller than the one of the bending magnets. With these parameters we evaluated a spin rotation of $\approx 0.25^\circ$ due to the magnetic component and of $\approx 7^\circ$ due to the electrostatic component. Note that the longitudinal polarization is, by definition, referred to the muon velocity, while the polarization we are interested in is the one in the beam direction, our natural quantization axis. Therefore the spin rotation results in a depolarizing effect of $\approx 0.8 \%$; this is confirmed by a numerical integration of the Thomas and Lorentz equations along the MEG beam line.

2.3 Depolarization during the muon moderation and stopping processes.

The largest muon depolarization effect is expected to take place in the MEG muon stopping target. The behaviour of positive muons in matter is extensively discussed in the literature (for a review H. et al. [1975]). After a rapid moderation and thermalization of muons in matter, muonium (μ^+e^-) is formed and further thermalized by collisions. The muon polarization is unaffected during the muonium formation and thermalization and subsequent decay. Muonium interaction with the magnetic field in vacuum is described by a hyperfine Hamiltonian, which includes the muon-electron spin-spin interaction and the Larmor interaction of both spins with the external field. On the basis defined by the total spin S and by its projection along the quantization axis S_z , the muonium wavefunction is a superposition of a triplet state ($S = 1$) and of a singlet state ($S = 0$). If one assumes muons to be fully polarized in the longitudinal direction when they enter the target and electrons in the target to be unpolarized, the initial state of the muonium formation is a 50 % – 50 % mixture of the state ($S = 1, S_z = -1$) and the combination of ($S = 1, S_z = 0$) and ($S = 0, S_z = 0$). The coefficients of this combination and their time evolution

can be calculated as functions of the ratio $x = B/B_0$, where B is the external magnetic field and $B_0 = 0.1585$ T. While the ($S = 1, S_Z = -1$) component is a pure state and is constant, the other oscillates with time; one can calculate its time average, which translates into an average longitudinal polarization given by:

$$\langle P_{\parallel}(x) \rangle = \frac{1}{2} \left(1 + \frac{x^2}{1+x^2} \right) \quad (4)$$

Since x at the position of the MEG target is $x \approx 7.9$, we obtain an average residual polarization of 99.2 %: any depolarizing effect is quenched by the strong magnetic field. However, muons are propagating in a dense medium and not in vacuum; therefore the muonium interaction with the material medium should be taken into account, making a detailed calculation impossible. We therefore used available experimental data, i.e. direct measurements of the muon residual polarization after crossing different targets immersed in external magnetic fields. The MEG target is a layered structure of polyethylene and polyethylene terephthalate (PET), for which no direct measurement is available; we assume this material to behave like polyethylene Swanson [1958], Buhler et al. [1965a,b]. With zero magnetic field, the residual muon polarization is (67.1 ± 2.0) % and reaches ≈ 100 % for increasing magnetic fields. Fig. 1 shows the value of muon residual polarization as a function of the magnetic field intensity (adapted from Buhler et al. [1965b]): the polarization saturates at ≈ 100 % for a magnetic field intensity of ≈ 4 kG, while the central value of the COBRA magnetic field is > 12 kG. So, we can assume that even in our case the

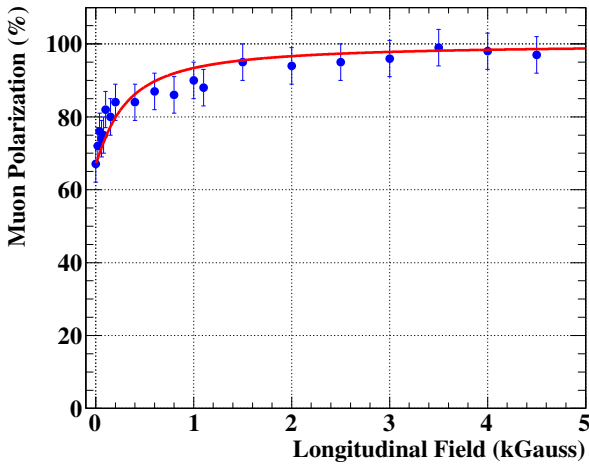


Fig. 1 Muon residual polarization after the muons stop in a polyethylene target, as a function of the external magnetic field (adapted from Buhler et al. [1965b]).

strong magnetic field quenches any depolarizing effect.

Table 1 Summary of main depolarizing effects (%).

Source	(%)
Multiple scattering in the production target	0.3
Cloud muons	4.5
Muon transport along the beam line	0.8
Muon interactions with the MEG target	negligible
Muon angular spread at the target	3.0
Total	8.6

The last point to be addressed is that muons reach the target centre under different angles within a $\approx 1 \times 1$ cm² beam spot. This angular spread corresponds to an apparent depolarization, since P_{μ} does not coincide with P_{μ}^z . Using the full MEG Monte Carlo simulation we evaluated that the angular divergence at the target corresponds to a cone of $< 20^\circ$ opening angle, corresponding to ≈ 3 % apparent depolarization.

2.4 Total depolarization

In conclusion, the main depolarizing effects are due to cloud muons and beam divergence. The average final polarization along the beam axis (z) is:

$$\langle P_{\mu}^z \rangle = (-0.91 \pm 0.03) \quad (5)$$

where the systematic uncertainty takes into account the uncertainties in this computation. The various contributions are listed in Table 1.

3 Expected Michel positron spectrum from polarized muons

The angular distribution of Michel positrons, including the radiative corrections Kuno and Okada [2001], was calculated in detail by several authors. The bidimensional energy-angular distribution for polarized muons decaying at rest takes the following form:

$$\frac{d^2\Gamma(\mu \rightarrow e^+ \nu \bar{\nu})}{dx d\cos\theta_e} = \frac{m_{\mu}^5 G_F^2}{192\pi^3} x^2 \left[(3 - 2x) + P_{\mu} \cos\theta_e (2x - 1) \right] + R.C. \quad (6)$$

where R.C. stands for “Radiative Corrections”, P_{μ} is the muon polarization, $x = 2E_{e^+}/m_{\mu}$ ($0 \leq x \leq 1$) and θ_e is the angle formed by the positron momentum vector and the muon spin vector. We show in Fig. 2 the angular distribution in the angular range $60^\circ \div 120^\circ$ for different values of x . The differential decay width for $x = 1$ at $\theta_e = 70^\circ$ is about twice that at $\theta_e = 110^\circ$. Inspection of Fig. 2 shows that detectable effects are expected in the MEG data sample, even if the MEG apparatus is not the best suited for polarization measurements due to the relatively small angular range, centred around $\theta_e = 90^\circ$.

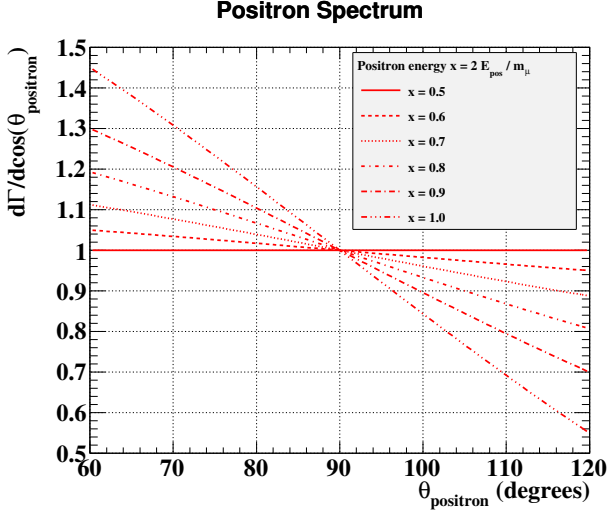


Fig. 2 Angular distributions of Michel positrons referred to the muon spin direction, for full polarization ($P_\mu = 1$) and for six different values of x , as given by formula (6). The vertical scale is in arbitrary units and normalized to 1 for $\theta_e = 90^\circ$.

4 Results of the measurement

4.1 Generalities

In the previous section we showed that polarization effects can be observed in the angular distributions of high-energy positrons from Michel decays. In addition to that, the distribution of high-energy photons from Radiative Muon Decay (RMD) is expected to be affected by the polarization; however its associated error is very large, because of the intrinsic uncertainties in the analysis method, mainly related to the determination of the photon emission angle, and because of the presence in this data sample of a large background of photons from other sources (e.g. bremsstrahlung, annihilation in flight, pile-up of lower energy gamma's ...). We will therefore disregard this item.

It is important to note that in formula (6) the quantization axis is the muon spin direction; however, surface muons are expected to be fully polarized in the backward direction, i.e. along the negative z -axis. Therefore, the polar angle θ in the MEG reference frame is related to θ_e in (6) by $\theta = 180^\circ - \theta_e$. Hence, the excess in the theoretical angular distribution (6) for $\theta_e < 90^\circ$ corresponds to an excess for $\theta > 90^\circ$ in the experimental angular distribution, i.e. on the US-side.

A very powerful way to study the muon polarization is to compare the energy spectra, integrated over the angular acceptance, on the US ($(dN/dE_{e^+})_{US}$) and on the DS ($(dN/dE_{e^+})_{DS}$) sides. We show in Fig. 3 as a function of positron energy E_{e^+} between 45 MeV and 53 MeV the asymmetry:

$$A(E_{e^+}) = \frac{((dN/dE_{e^+})_{US} - (dN/dE_{e^+})_{DS})}{((dN/dE_{e^+})_{US} + (dN/dE_{e^+})_{DS})} \quad (7)$$

in the upper part and the ratio:

$$R(E_{e^+}) = \frac{(dN/dE_{e^+})_{US}}{(dN/dE_{e^+})_{DS}} \quad (8)$$

in the lower part for three representative polarization values: 0 (red dotted line), -0.5 (black dashed line) and -1 (blue continuous line).

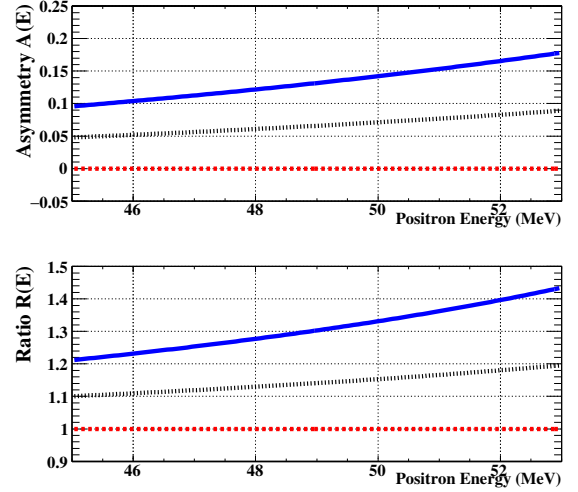


Fig. 3 The asymmetry (7) (upper plot) and the ratio (8) (lower plot) as a function of the positron energy E_{e^+} , for three representative polarization values: 0 (red dotted line), -0.5 (black dashed line) and -1 (blue continuous line). All spectra are obtained by integrating the 2-D (energy, angle) distributions over the MEG angular range.

4.2 Analysis of Michel positrons

Experimentally measured angular distributions result from the folding of the theoretical distributions and of the detector response, acceptance and thresholds, whose non-uniformities can mimic angular asymmetries or create fictitious ones. Topological requirements and quality cuts needed to define and fit charged particle tracks also introduce angle-dependent non-uniformities. In particular, the tracking algorithm has a lower efficiency for positrons emitted with small longitudinal momenta, resulting in a dip in the angular distribution of Michel positrons for $\theta \approx 90^\circ$ (see later Fig. 6). MEG positrons are mainly produced by muon decays in the stopping target, with a significant fraction ($\sim 20\%$) decaying off-target, in beam elements or in the surrounding helium gas. These decays predominantly take place on the DS-side, diluting the experimental US-DS asymmetry. However, this contribution can be minimized by requiring the reconstructed positron decay vertex to lie within the target volume. As a consequence, an analytical prediction of the experimental distribution is rather complicated; hence, we de-

cided to measure the muon polarization by means of two different analysis strategies:

- in the first one, we compared the energy integrated experimental angular distribution of Michel positrons with that obtained by a detailed Geant3-based MC simulation of those events, as seen in the MEG detector, with the muon polarization as a free input parameter;
- in the second one, we measured the US-DS asymmetry $A(E_{e^+})$ and the ratio $R(E_{e^+})$ as a function of positron energy and fit them with the expected phenomenological forms, after unfolding the detector acceptance and response.

4.2.1 MC simulation

The MEG MC simulation is described in details in Adam et al. [2010] and Cattaneo et al. [2011]. Michel positrons were generated in the stopping target (a full simulation of the muon beam up to the stopping target is also possible, but brings no significant advantage in this case) with a minimum energy of 40 MeV and a muon polarization P_μ varying between 0 and -1 in steps of 0.1. A smaller step size of 0.05 was used between -0.8 and -1 , close to the expected value (section 2). Separated samples of MC events were produced for each polarization value and the positron energy and direction were generated according to the theoretical energy-angle distribution corresponding to this polarization. Positrons were individually followed along the apparatus and their hits in the tracking system and on the timing counters were recorded; a simulation of the electronic chain converted these hits into anodic and cathodic signals which were processed by the same analysis algorithms used for real data. Modifications of the apparatus configuration during the whole period of data taking were simulated in detail, following the information recorded for each run in the experiment database. The position and spatial orientation of the target varied slightly each year, as well as trigger and acquisition thresholds, beam spot centre and size and the drift chamber alignment calibration constants. Some of the drift chambers suffered from instabilities, with a time scale from days to weeks, with their supply voltages finally set to a value smaller than nominal. The supply voltage variations, chamber by chamber, were also followed in the simulation on a run by run basis. However, voltage instabilities do not significantly affect the polarization measurement. Since drift chamber wires run along the z -axis, a non operating chamber produces the same effect on US and DS if the beam is perfectly centred on the target, while it gives a second order contribution to the US-DS asymmetry when the beam is not perfectly centred. The number of MC events generated using the global configuration (target position, alignment ...) corresponding to a given year is proportional to the actual amount of data collected in that year.

4.2.2 Data sample

The data sample contains the events collected between 2009 and 2011 by a pre-scaled trigger requiring only a timing counter hit above the threshold (so called “trigger 22”). The analysis procedure requires an accurate pre-selection of good quality tracks: strict selection cuts are applied in order to single out tracks with good angular and momentum resolutions, well matched with at least one timing counter hit and with the decay vertex reconstructed within the target volume. A fiducial volume cut is included to avoid efficiency distortions at the borders of the acceptance. The sample and the selection criteria are essentially those used to identify Michel events for the absolute normalization of the MEG data (see Adam et al. [2011a, 2013b]). About 37k (2009), 65k (2010) and 115k (2011) positron tracks passed all selection cuts, for a total of about 2.1×10^5 events. The same criteria were applied to the MC tracks; about 1.3×10^5 events passed all selections for each polarization value.

4.2.3 Comparison between MC and data

The comparison between the reconstructed positron vertex coordinates x , y and z for data (blue points) and MC (red line, normalized to the data) are shown in Fig. 4, top and bottom left; at the bottom right of this Figure we show the same comparison for the reconstructed azimuthal angle ϕ at the positron emission point. We also show in Fig. 5 the compar-

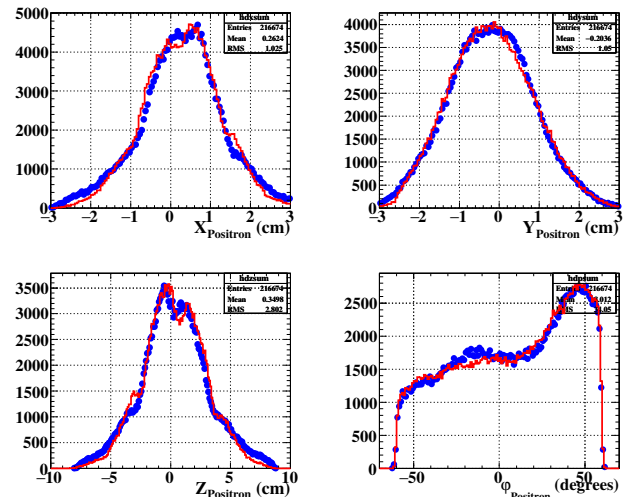


Fig. 4 Comparison between the reconstructed vertex coordinates x , y and z and the azimuthal ϕ angle, for real (blue points) and simulated data (red line, normalized to the data). The polarization of the MC sample is -0.85 ; the distributions corresponding to different polarizations are almost identical.

ison between data (blue points) and MC (red line) positron energy spectra on the US (left) and DS (right) sides, both

on linear (upper part) and on logarithmic (lower part) scale. The agreement is generally good for all variables, with some small discrepancies, visible in the logarithmic energy spectra, for $E_{e^+} > 53$ MeV, where the MC does not perfectly reproduce the tails of the experimental resolution, and for $E_{e^+} < 46$ MeV, where significant effects induced by threshold and acceptance are present. Such effects are particularly

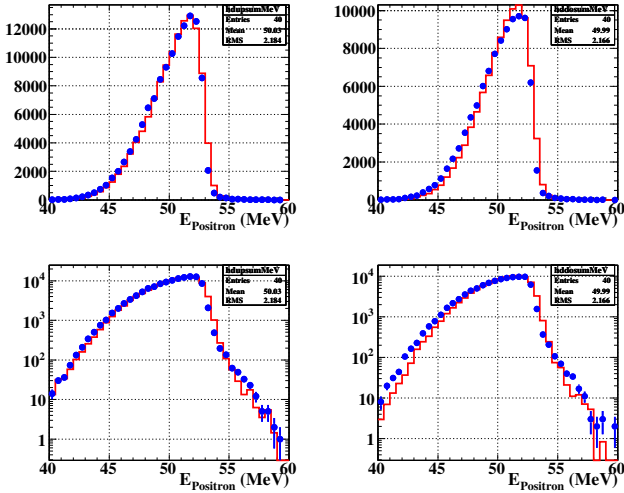


Fig. 5 Comparison between data (blue points) and MC (red line, normalized to the data) positron energy spectra for the US (left) and DS (right) sides, on linear (upper plots) and on logarithmic scale (lower plots).

relevant in the sample of year 2010, when the beam spot was displaced with respect to the target centre by ~ 1 cm. (See section 4.2.7 dedicated to the analysis of systematic uncertainties.)

The general agreement between data and MC for all reconstructed variables demonstrates our ability to correctly simulate the behaviour of the apparatus.

4.2.4 Efficiency correction for MC and data

The efficiency for the full reconstruction of a positron event is composed of two parts: the absolute efficiency $\epsilon(\text{Track})$ for producing a track satisfying all trigger and software requirements and the relative efficiency $\epsilon(\text{TC}|\text{Track})$ of having a TC hit, given a track. Both efficiencies are functions of the positron energy and emission angles and can be different on the US and DS sides because of intrinsic asymmetries of the experimental apparatus.

The $\epsilon(\text{TC}|\text{Track})$ efficiency was separately computed for MC and real events. In the case of MC this calculation is straightforward. In the more complicate case of real data, we selected positrons collected by a different pre-scaled trigger (so called “trigger 18”) requiring only loose conditions on the number and the topological sequence of fired drift

chambers, and selected the fraction of tracks with an associated good TC hit within this sample. The MC and data $\epsilon(\text{TC}|\text{Track})$ efficiency matrices were then used to correct the θ angular distributions, $A(E_{e^+})$ and $R(E_{e^+})$.

The $\epsilon(\text{Track})$ efficiency was extracted from MC by looking at the reconstructed $R(E)$ in the MC sample generated with $P_\mu = 0$ and determining, year by year, an empirical correction function which makes this $R(E)$ always consistent with unity within the errors. We then applied the same correction functions to all MC samples and we checked that the polarization values extracted by fitting $A(E_{e^+})$ and $R(E_{e^+})$ were consistent with those generated. The correction functions were also applied to the data since the good agreement between MC and data shown in Fig. 4 and 5 gives us confidence of the correct apparatus response to positron events.

4.2.5 Results of first strategy: angular distribution

In Fig. 6 the comparison between the angular distributions of real data (blue points) and of MC events (red line, normalized to the data), after inserting the matching efficiency corrections, as a function of θ angle for two different polarization values is shown: $P_\mu = 0$ in the upper plot and $P_\mu = -0.85$ in the lower plot. According to (6) and to the

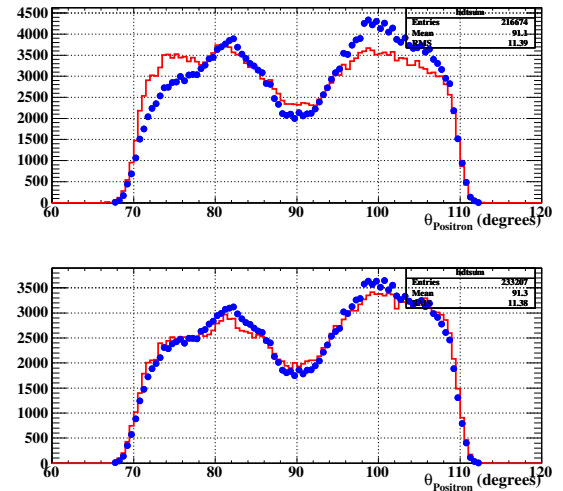


Fig. 6 Comparison between the angular distributions for simulated (red line) and measured (blue points) Michel positrons; $P_\mu = 0$ (upper plot) and $P_\mu = -0.85$ (lower plot). The polar angle θ is referred to the beam axis. Histograms are normalized to the data.

definition of θ , we expect to observe an asymmetric distribution for large values of the polarization, with an excess on the US-side ($\theta > 90^\circ$) and a symmetric distribution for null polarization. Fig. 6 shows a clear disagreement between data and MC for $P_\mu = 0$ and a good agreement for $P_\mu = -0.85$. The simulation well reproduces the US-DS asymmetry observed in the data, as well as the dip for $\theta \approx 90^\circ$. Angular

distributions for $P_\mu = -0.8$ and for $P_\mu = -0.9$ do not significantly differ from that shown for $P_\mu = -0.85$: the comparison between data and MC gives strong indications for a large polarization, $-(0.8 - 0.9)$, but it is not precise enough to single out a value of P_μ , with its uncertainty.

4.2.6 Results of second strategy: US-DS asymmetry and ratio

A quantitative estimate of the polarization can be obtained by studying the angle-integrated energy distributions $(dN/dE)_{US}$ and $(dN/dE)_{DS}$ on the US and DS sides. Formula (6) shows that the difference between the US and DS sides is (apart from higher order effects, like radiative corrections) due to the presence of a term proportional to $xP_\mu \cos \theta$. Since the sign of this term changes from US (where, according to our definition of polar angles, it is positive) to DS (where, with the same definition, it is negative), one expects that both the asymmetry $A(E_{e^+})$ and the ratio $R(E_{e^+})$ increase almost linearly with the positron energy. The slope of this dependence is $P_\mu \cos \theta$: one can therefore extract a polarization value by fitting the experimentally measured asymmetry and ratio and dividing the measured slope by the average value of $|\cos \theta| = 0.1762$ for the US and DS sections. The interval of the fit was restricted to (46 – 53) MeV to minimize possible distortions due to the energy-angle dependencies of the energy threshold and because formula (6) is meaningless for $E > 52.83$ MeV, i.e. $x > 1$. The expected plots for $A(E_{e^+})$ and $R(E_{e^+})$ are shown in Fig. 3. The experimental $A(E_{e^+})$ and $R(E_{e^+})$ were separately determined year by year and summed. The fit results for the full data sample are shown in Fig. 7; the average value of the two fits is

$$P_\mu = -0.846 \pm 0.027 \quad (9)$$

where the quoted error is only statistical. The average $\chi^2/d.o.f.$ of the fits is 2.3, mainly determined by the points close to the threshold. In Fig. 8 we show the comparison between data (blue filled points) and MC generated with $P_\mu = -0.85$ (red open triangles) for $A(E_{e^+})$ (upper plot) and $R(E_{e^+})$ (lower plot) between 45 and 55 MeV: the agreement is quite good everywhere except above 53 MeV, where the MC is unable to reproduce the experimental resolution with sufficient accuracy. However, it should be noted that the energy region above 53 MeV does not affect the result, since the fit was limited to (46 – 53) MeV. We checked that these results do not depend on the fitting interval by eliminating one bin at the lower bound and/or one bin at the upper bound: in all cases the fit results agreed with (9) within the statistical error.

4.2.7 Systematic uncertainties

Various systematic uncertainties can produce sizable effects on this measurement. We single out five main possible sources:

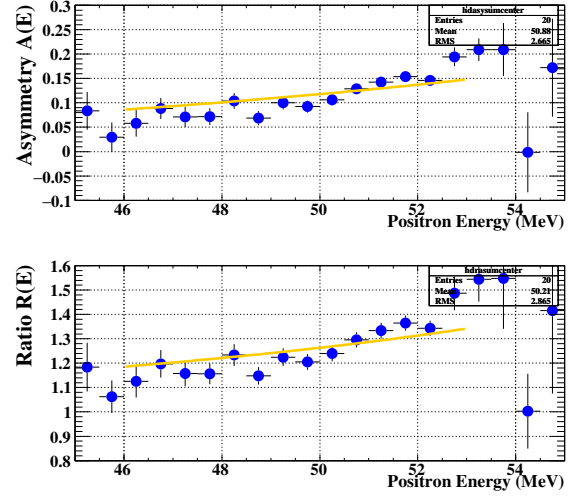


Fig. 7 Fit of $A(E_{e^+})$ (upper plot) and of $R(E_{e^+})$ (lower plot) as a function of the positron energy. The experimental data are corrected, year by year, by the MC-based tracking efficiency function. The fitting functions are obtained from the (6) distribution.

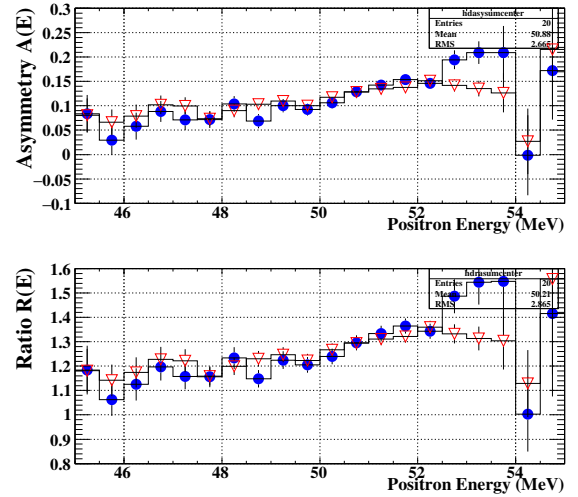


Fig. 8 Comparison between data (blue filled points) and MC for $P_\mu = -0.85$ (red open triangles). $A(E_{e^+})$ (upper plot) and $R(E_{e^+})$ (lower plot) between 45 and 55 MeV.

energy scale, angular bias, target position, MC-based efficiency corrections and threshold effects. The first three affect the shape of the spectra on the US and DS sides and the evaluation of the relative efficiency $\epsilon(TC|Track)$ from data; the fourth determines the absolute tracking efficiency and the fifth can alter the $A(E_{e^+})$ and $R(E_{e^+})$ fits in the bins close to the lower bound of the fit interval.

- 1) Energy scale. The energy scale and resolution are determined in MEG, as discussed in Adam et al. [2011a], by fitting the Michel positron energy spectrum with the convolution of the theoretical spectrum (including radiative corrections) of the detector acceptance and of a resolution curve, in the form of a partially constrained

triple Gaussian shape. The position of the Michel edge, used as a reference calibration point, is determined with a precision of $\delta E_{e^+} \sim 30$ keV. The effect of this uncertainty was evaluated by varying the reconstructed energy of our events by a factor $(1 \pm \delta E_{e^+}/\bar{E}_{e^+})$, where $\bar{E}_{e^+} = 52.83$ MeV is the position of the Michel edge, and repeating the analysis. The polarization value determined by the average of $A(E_{e^+})$ and $R(E_{e^+})$ fits increases by 0.0027 when $\delta E_{e^+}/\bar{E}_{e^+}$ is added and decreases by -0.0046 when $\delta E_{e^+}/\bar{E}_{e^+}$ is subtracted.

- 2) Angular bias. The angular resolution is determined by looking at tracks crossing the chamber system twice (double turn method), as discussed in Adam et al. [2010, 2011a]. The uncertainty on the θ and ϕ scales varies between 1 and 3 mrad. The effect of this uncertainty on the angular scale was (conservatively) evaluated by modifying both the reconstructed polar angles by ± 3 mrad and repeating the analysis. The measured polarization decreases (increases) by -0.012 ($+0.023$).
- 3) Target position. The target position with respect to the centre of the COBRA magnet is measured by means of an optical survey and checked by looking at the distribution of the positron vertex of reconstructed tracks. The discrepancies between the two methods are at the level of a fraction of a mm. Since in our analysis we require that the reconstructed positron vertex lies within the target ellipse, an error on the target position can alter the positron selection. We assumed a conservative estimate of a target position uncertainty of ± 1 mm on all coordinates and, as previously, added or subtracted it and repeated the analysis. The effect was to decrease (increase) the polarization by -0.019 (0.005).
- 4) MC-based corrections. The MC corrections, inserted to take into account the absolute tracking efficiency, are based on the position of the target as measured by the optical survey and on the nominal location of the beam centre. A variation of these parameters produces a variation on the correction functions, applied year by year to MC and data. We estimated the size of this effect by generating MC samples with a displaced beam and target (± 1 mm shift as previously) and null polarization and determined new tracking efficiency correction functions. Such functions were then applied to the data and MC: the measured polarization decreased (increased) by -0.034 (0.028).
- 5) Threshold effects. The response of the MEG tracking system close to the momentum threshold ($E_{e^+} \approx 45$ MeV) depends in general on the polar angles and can be significantly distorted when the beam and target are not centred, causing fictitious differences between the US and DS sides. In 2010 the beam was displaced by more than 10 mm in the x -direction and about 6 mm in the y -direction producing an asymmetric US-DS energy thresh-

Table 2 Main systematic uncertainties and their effect on polarization.

Source	(ΔP)
Energy scale	($+0.0027, -0.0046$)
Angular scale	($+0.023, -0.012$)
Target position	($+0.005, -0.019$)
Tracking efficiency	($+0.028, -0.034$)
Energy threshold	-0.034
Total (in quadrature)	($+0.037, -0.053$)

old, with the DS spectrum systematically higher than the US one for $E_{e^+} < 47$ MeV. The beam and target displacement were introduced in the MC, but the simulation for 2010 did not result in a perfect agreement with the data in the region close to the energy threshold. We then estimated the systematic effect due to the angular dependence of the energy threshold by removing the 2010 sample from the fit: the polarization decreases by -0.034 , a difference larger than the statistical error. Note that the average $\chi^2/d.o.f.$ of the fit improved significantly from 2.3 to 0.8. An improved fit quality was observed also on MC events by removing the simulated data corresponding to the year 2010 configuration.

The effects of the various systematic uncertainties and the global systematic uncertainty calculated by their addition in quadrature are reported in Tab.2.

Combining the fit results in (9) with the numbers reported in Tab.2 we can state that the muon residual polarization in the MEG experiment is:

$$P_\mu = -0.85 \pm 0.03 \text{ (stat)} \text{ }^{+0.04}_{-0.05} \text{ (syst)} \quad (10)$$

5 Summary and conclusions

We measured the residual muon polarization P_μ in the MEG experiment by studying the energy-angle distribution of Michel positrons collected during three years of data taking. We obtained:

$$P_\mu = -0.85 \pm 0.03 \text{ (stat)} \text{ }^{+0.04}_{-0.05} \text{ (syst)} \quad (11)$$

The measured value is in agreement with the calculation of the depolarizing effects due to the muon spin interactions during the production and the propagation through the apparatus up to the stopping target, based on the SM prediction of positive surface muons, produced fully polarized in the direction opposite to the beam direction. Moreover, the Michel positron angular distribution and the US - DS asymmetry of the positron energy spectra are well reproduced by a complete simulation of the positron detection in the MEG set-up when a muon polarization $P_\mu = -0.85$ is used as an input parameter in the Monte Carlo calculation. This result is important to allow a precise calculation of the Radiative Muon

Decay branching ratio and energy-angle distribution in the kinematic region where it represent a background source to the search for $\mu^+ \rightarrow e^+\gamma$ and can be used as a tool for the absolute normalization of the MEG experiment.

6 Acknowledgements

We are grateful for the support and cooperation provided by PSI as the host laboratory and to the technical and engineering staff of our institutes. This work is supported by SNF grant 200021_137738 (CH), DOE DEFG02-91ER40679 (USA), INFN (Italy) and MEXT KAKENHI 22000004 (Japan). Partial support of the Italian Ministry of University and Research (MIUR) grant RBFR08XWGN, Ministry of University and Education of the Russian Federation and Russian Fund for Basic Research grants RFBR 14-22-03071 are acknowledged.

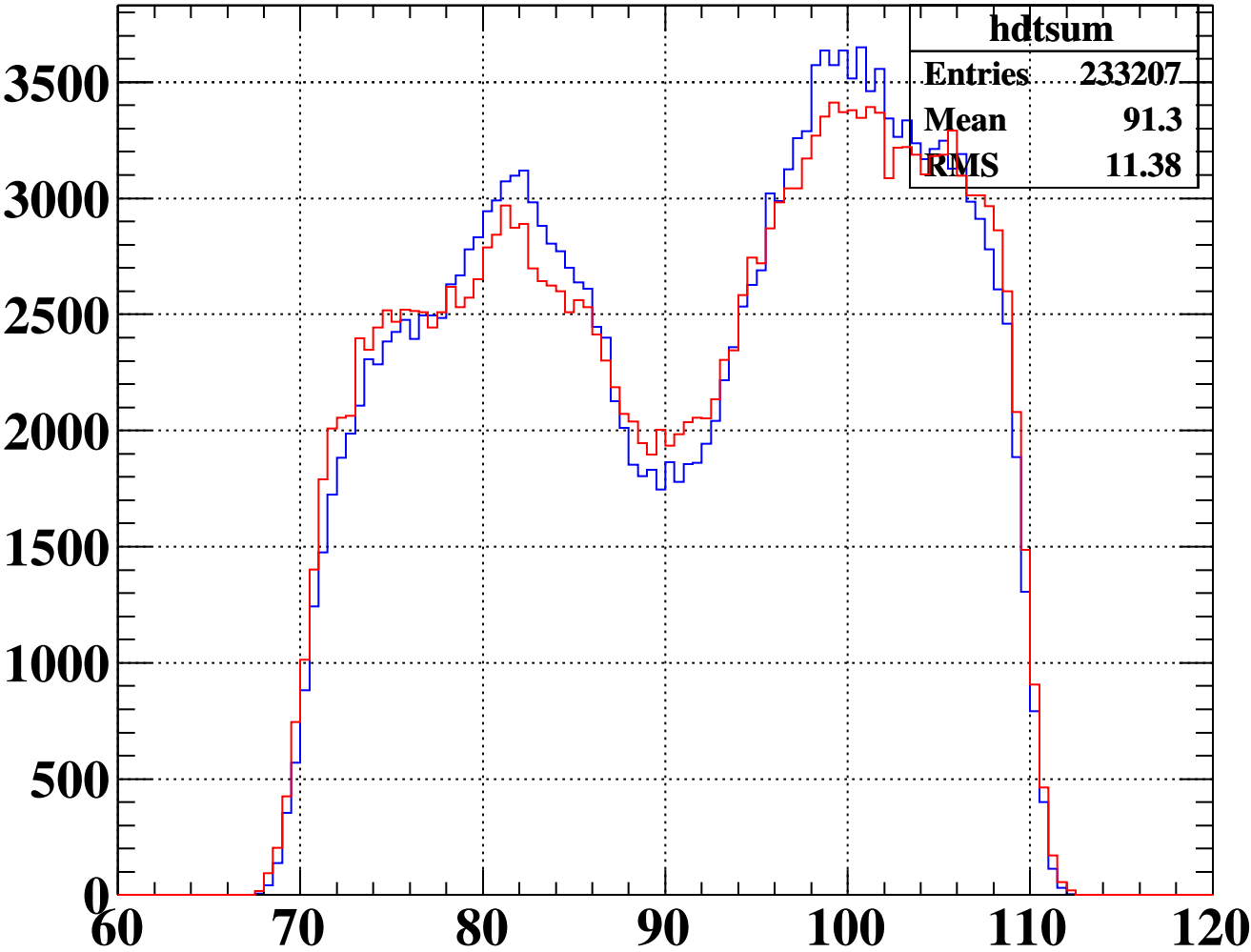
References

aea.web.psi.ch/beam2lines/beam.pie5.html.

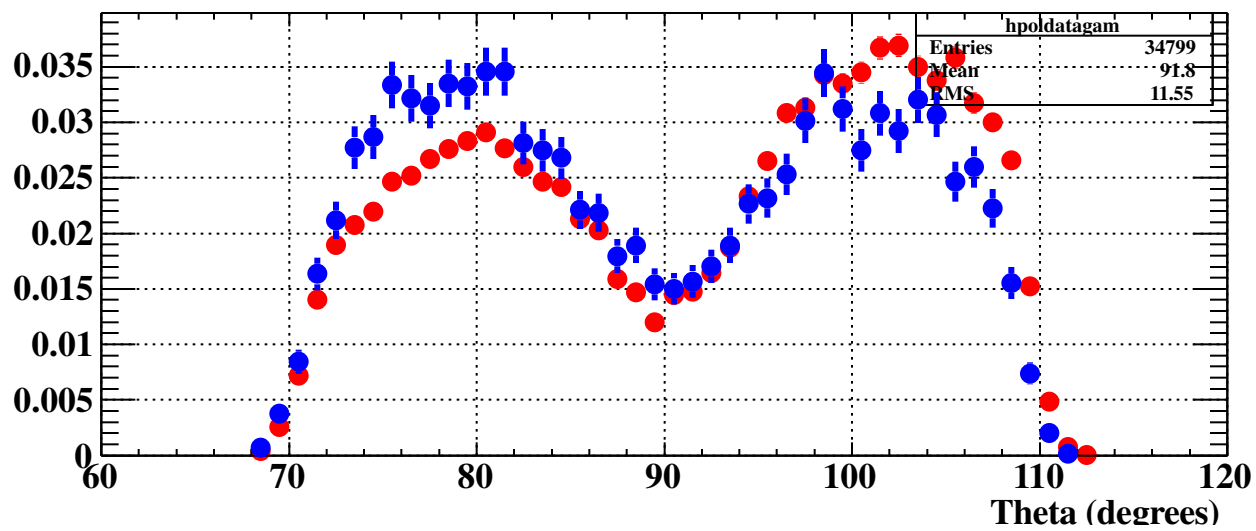
- J. Adam et al. The MEG detector for $\mu^+ \rightarrow e^+\gamma$ decay search. *Eur. Phys. J. C*, 73:2365, 2013a. doi: 10.1140/epjc/s10052-013-2365-2. www.psi.ch.
- J. Adam et al. A limit for the $\mu^+ \rightarrow e^+\gamma$ decay from the MEG experiment. *Nucl. Phys.*, B834:1–12, 2010. doi: 10.1016/j.nuclphysb.2010.03.030.
- J. Adam et al. New limit on the lepton-flavour violating decay $\mu^+ \rightarrow e^+\gamma$. *Phys. Rev. Lett.*, 107:171801, 2011a.
- J. Adam et al. New constraint on the existence of the $\mu^+ \rightarrow e^+\gamma$ decay. *Phys. Rev. Lett.*, 110:201801, 2013b.
- A. Yamamoto et al. A thin superconducting solenoid magnet for particle physics. *Appl. Supercond., IEEE Trans. on*, 12:438–441, 2002.
- W. Ootani, W. Odashima, S. Kimura, T. Kobayashi, Y. Makida, T. Mitsuhashi, S. Mizumaki, R. Ruber, and A. Yamamoto. Development of a thin-wall superconducting magnet for the positron spectrometer in the MEG experiment. *Appl. Supercond., IEEE Trans. on*, 14(2):568–571, June 2004. ISSN 1051-8223. doi: 10.1109/TASC.2004.829721.
- M. Hildebrandt. The drift chamber system of the MEG experiment. *Nucl. Instr. Methods Phys. Res., Sect. A*, 623(1):111 – 113, 2010. ISSN 0168-9002. doi: DOI:10.1016/j.nima.2010.02.165. URL www.sciencedirect.com/science/article/B6TJM-4YH4PT3-J/2/ed88926b9cd6200dc6bf7d367d20e19.
- S. Dussoni and M. De Gerone and F. Gatti and R. Valle and M. Rossella and R. Nardó and P.W. Cattaneo. The Timing Counter of the MEG experiment: design and commissioning. *Nucl. Instr. Methods Phys. Res., Sect. A*, 617(1-3):387 – 390, 2010. ISSN 0168-9002. doi: DOI:10.1016/j.nima.2009.08.089. URL www.sciencedirect.com/science/article/B6TJM-4X6FNFV-5/2.
- M. De Gerone, S. Dussoni, K. Fratini, F. Gatti, R. Valle, et al. Development and commissioning of the Timing Counter for the MEG Experiment. *IEEE Trans. Nucl. Sci.*, pages 379–388, 2012. doi: 10.1109/TNS.2012.2187311.
- M. De Gerone, S. Dussoni, K. Fratini, F. Gatti, R. Valle, et al. The MEG timing counter calibration and performance. *Nucl. Instrum. Meth.*, A638:41–46, 2011. doi: 10.1016/j.nima.2011.02.044.
- R. Sawada. Performance of liquid xenon gamma ray detector for MEG. *Nucl. Instr. Methods Phys. Res., Sect. A*, 623(1):258 – 260, 2010. ISSN 0168-9002. doi: DOI:10.1016/j.nima.2010.02.214. URL www.sciencedirect.com/science/article/B6TJM-4YH99K0-11/.
- Satoshi Mihara. MEG liquid xenon detector. *J. Phys. Conf. Ser.*, 308:012009, 2011. doi: 10.1088/1742-6596/308/1/012009.
- L. Galli, F. Cei, S. Galeotti, Magazzù C., D. Nicolò, G. Signorelli, and M. Grassi. An FPGA-based trigger system for the search of $\mu^+ \rightarrow e^+\gamma$ decay in the MEG experiment. *J. Instrum.*, 8:P01008, 2013. doi: 10.1088/1748-0221/8/01/P01008.
- L. Galli, A. Baldini, P.W. Cattaneo, F. Cei, M. De Gerone, S. Dussoni, et al. Operation and performance of the trigger system of the MEG experiment. *J. Instrum.*, 9: P04022, 2014. doi: 10.1088/1748-0221/9/04/P04022.
- S. Ritt. The DRS chip: cheap waveform digitizing in the GHz range. *Nucl. Instr. Methods Phys. Res., Sect. A*, 518(1-2):470–471, Feb 2004. URL www.sciencedirect.com/science/article/B6TJM-4BT3HYY-4V/.
- S. Ritt, R. Dinapoli, and U. Hartmann. Application of the DRS chip for fast waveform digitizing. *Nucl. Instr. Methods Phys. Res., Sect. A*, 623(1):486 – 488, 2010. ISSN 0168-9002. doi: DOI:10.1016/j.nima.2010.03.045. URL www.sciencedirect.com/science/article/B6TJM-4YJCKNT-R/2.
- A. Baldini et al. A radioactive point-source lattice for calibrating and monitoring the liquid xenon calorimeter of the MEG experiment. *Nucl. Instr. Methods Phys. Res., Sect. A*, 565(2):589 – 598, 2006. ISSN 0168-9002. doi: DOI:10.1016/j.nima.2006.06.055. URL www.sciencedirect.com/science/article/B6TJM-4KDBJ0M-9/2.
- J. Adam et al. Calibration and monitoring of the MEG experiment by a proton beam from a Cockcroft-Walton accelerator. *Nucl. Instr. Methods Phys. Res., Sect. A*, 641: 19–32, 2011b.
- A. E. Ritt. A high stopping density μ^+ beam. *Nucl. Instr. Methods Phys. Res., Sect. A*, 135:39, 1976.
- O.B. Van Dyck, E.W. Hoffman, R.J. Macek, G. Sanders, R.D. Werbeck, et al. 'Cloud' and 'surface' muon beam characteristics. *IEEE Trans. Nucl. Sci.*, 26:3197–3199, 1979. doi: 10.1109/TNS.1979.4329982.

-
- J. D. Jackson. *Classical Electrodynamics*. Wiley & Sons, 1998.
- Brewer J. H., others in Hughes V. W., and C.S. Wu. *Muon Physics*, chapter vol III and I. Academic Press, New York, 1975.
- R. A. Swanson. Depolarization of positive muons in condensed matter. *Phys. Rev.*, 112(2):580–586, 1958.
- A. Buhler et al. Measurements of muon depolarization in several materials. *Nuovo Cimento*, 39:824, 1965a.
- A. Buhler et al. Study of the quenching of muon depolarization in several materials as a function of externally applied magnetic fields. *Nuovo Cimento*, 39:812, 1965b.
- Y. Kuno and Y. Okada. Muon decay and physics beyond the standard model. *Rev. Mod. Phys.*, 73(1):151–202, 2001. doi: 10.1103/RevModPhys.73.151.
- P.W. Cattaneo, F. Cei, R. Sawada, M. Schneebeili, and S. Yamada. The architecture of MEG simulation and analysis software. *Eur. Phys. J. Plus*, 126(7):1–12, 2011. doi: 10.1140/epjp/2011-11060-6.

hdtsum



Event Fraction



Event Fraction

